

*promoting access to White Rose research papers*



**Universities of Leeds, Sheffield and York**  
**<http://eprints.whiterose.ac.uk/>**

---

This is the author's pre-print version of an article published in the **Journal of Hydrology**

White Rose Research Online URL for this paper:

<http://eprints.whiterose.ac.uk/id/eprint/76080>

---

**Published article:**

Carrivick, JL, Brown, LE, Hannah, DM and Turner, AGD (2011) *Numerical modelling of spatio-temporal thermal heterogeneity in a complex river system*. Journal of Hydrology, 414-41. 491 - 502. ISSN 0022-1694

<http://dx.doi.org/10.1016/j.jhydrol.2011.11.026>

---

1 Numerical modelling of spatio-temporal thermal  
2 heterogeneity in river systems

3  
4 *Jonathan L. Carrivick<sup>1\*</sup>, Lee E. Brown<sup>1</sup>, David M. Hannah<sup>2</sup> and Andy G.D. Turner<sup>1</sup>*

5  
6  
7 1. School of Geography, University of Leeds, Leeds, LS2 9JT. UK

8 2. School of Geography, Earth and Environmental Science, University of Birmingham, Birmingham,  
9 B15 2TT. UK.

10  
11 \* Author for correspondence

12 E: [j.l.carrivick@leeds.ac.uk](mailto:j.l.carrivick@leeds.ac.uk)

13 T: (+44) 0113 343 3324

14 F: (+44) 0113 343 3308

15  
16  
17 Running title: Modelling river temperature dynamics  
18  
19

1 **Abstract**

2

3 Accurate quantification and effective modelling of water temperature regimes is fundamental to  
4 underpin projections of future Arctic river temperature under scenarios of climate and hydrological  
5 change. We present results from a deterministic two-dimensional hydrodynamic model coupled with a  
6 heat transfer model that includes horizontal advection and vertical water surface energy fluxes. Firstly,  
7 we model longitudinal, lateral and temporal thermal heterogeneity of a braided reach of an Arctic river;  
8 Kårsajökk, Sweden. Model performance was assessed against water temperature data collected at 11  
9 monitoring sites for two independent one week time periods. Overall, model performance was strongest  
10 ( $r$  values  $> 0.9$ ,  $RMSEs \sim 0.6$  °C and  $ME < 0.4$  °C) for main channel sites with relatively deep fast-flows  
11 where water temperature was comparatively low and stable. However, model performance was poorer  
12 for sites characterized by shallow and/or temporarily-stagnant streams at the lateral margins of the  
13 braidplain, where a lag of 60 – 90 minutes persisted between the modelled and measured water  
14 temperatures. Secondly, we present automated statistical analyses and quantify channel thermal  
15 connectivity and complexity. Our results enable us to suggest that with further development our  
16 modelling approach offers potentially new opportunities for scenario-based predictions of response to  
17 environmental change and to assess anthropogenic impacts on water temperature.

18

19 **Keywords**

20

21 Water temperature, hydrodynamic model, heat budget, heat transport

22

23

24

## 1 **Introduction**

2

3 Water temperature is regarded widely as a ‘master’ water quality variable in aquatic systems due to its  
4 influence on a host of physical, chemical, and biological processes (Hawkins et al., 1997; Hannah *et al.*,  
5 2008). The study of thermal variability in rivers has a long history (Webb et al., 2008) but aquatic  
6 scientists still encounter problems in quantifying river thermal regime dynamics accurately. Current  
7 understanding of river temperature variability revolves largely around data collected from single sites.  
8 Whilst some researchers have adopted multi-site temperature recording campaigns to widen the scale of  
9 investigation (e.g. Arscott et al., 2001; Brown et al., 2008), these approaches poorly represent high-  
10 resolution (metre-scale) lateral and longitudinal thermal dynamics. Remote sensing approaches, such as  
11 thermal infra-red imagery, have yielded some success in characterizing the spatial heterogeneity of river  
12 thermal characteristics (Loheide and Gorelick, 2006; Tonolla et al., 2010) but suffer from limited  
13 temporal replication due to the expense of data acquisition and time-intensive processing (Cardenas et  
14 al., 2005).

15

16 Previous studies have shown the potential to model river thermal dynamics from hydroclimatological,  
17 i.e. river discharge, water temperature and meteorological data collected at single sites (Sinokrot and  
18 Stefan, 1993; Caissie et al., 2005). However, the introduction of low cost, miniature digital water  
19 temperature dataloggers (Webb et al., 2008), the increase in usability of differential Global Positioning  
20 Systems (dGPS) to rapidly create digital elevation models (DEMs), and the development of ‘two-  
21 dimensional’, or ‘distributed’ hydrodynamic models that are able to include water column temperature  
22 have yet to be exploited jointly for analyzing and understanding the connectivity and spatio-temporal  
23 heterogeneity of river thermal regimes. New technological solutions incorporating these elements offer  
24 the potential to: provide combined high spatial (metre-scale) and temporal (sub-hourly) resolution  
25 thermal data to inform accurate environmental impact studies (Caissie et al., 2005), provide the means  
26 to incorporate thermal heterogeneity into the planning stage of river remediation schemes (e.g. Young

1 and Collier, 2009; Hester and Gooseff, 2010), and predict river ecosystem responses to environmental  
2 change (Durance and Ormerod, 2007).

3

4 High-latitude environments are considered to be at severe risk of major changes due to climate change  
5 (e.g. Schiermeier, 2006). General circulation models of the climate system suggest above global-average  
6 rates of future warming in the Arctic, which will affect glacier mass-balance and, in turn, proglacial  
7 river system hydrology (Milner et al., 2009). The structural and functional biological characteristics of  
8 glacier-fed river ecosystems are known to be strongly influenced by water temperature (Hannah et al.,  
9 2007; Brown et al., 2007) but there have been few studies of the thermal regime of Arctic river systems  
10 (Brown and Hannah, 2007; Lammers et al., 2007). Thus, accurate quantification of present-day thermal  
11 regimes, coupled with computationally efficient solutions for predicting future change, is fundamental  
12 to underpin efforts to understand the wider implication of Arctic climate change.

13

14 This paper reports a study of spatio-temporal water temperature dynamics undertaken in Arctic  
15 Sweden. This is the first application of a two-dimensional heat transport model for rivers and therefore  
16 this study aims to: (i) present the two-dimensional heat transport model; (ii) assess the performance of  
17 this model in a variety of channel types and under a variety of weather conditions; iii) use this model as  
18 a tool to examine spatial and temporal patterns in water temperature heterogeneity, and iv) to use this  
19 model to infer processes of heat advection and dispersion in rivers.

## 20 **Study site and field methods**

21

22 Field data were obtained for a ~ 6 km part of the Kårsajöck River, which is in upper Kårsavagge near  
23 Abisko in Arctic Sweden (Fig. 1A). Kårsajöck is sourced primarily from Kårsaglaciaren, which is a ~ 2  
24 km<sup>2</sup> glacier. Kårsajöck runs through tundra above the tree line and therefore it is openly exposed to the  
25 atmosphere without trees or shading from other vegetation. Topographic shading is assumed to be

1 uniform across the reach since the valley floor is of gentle and uniform slopes and the river is central to  
2 the valley floor rather than abutted to hillslopes (Fig. 2B). The uppermost reach, which we focus on in  
3 this study, comprises a distinct main channel, a complex of braided channels and a longitudinally  
4 extensive lateral margin channel (Fig. 1C). The main channel is typically 4 m wide and 0.4 - 0.8 m deep,  
5 the depth varying diurnally due to snow and ice melt. Braided channels and the lateral margin channel  
6 are generally narrower and shallower than this although highly variable in space and through time.  
7 Across this upper reach channel substrate and (unstable) banks comprise cobble and gravel-sized clasts.  
8 The mid-reach of this part of Kårsajökk is a single-thread channel that runs within a 3 m – 6 m deep  
9 bedrock canyon between sites ‘Main 2’ and ‘Main 7’ (Fig. 1C). The lowermost (eastern) reach of this  
10 part of Kårsajökk; from site ‘Main 7’ eastwards, is a lake delta and the streams here have a silty-sand  
11 channel bed and grass-covered stable banks (Fig. 1C).

12

13 < [Figure 1 near here](#) >

14

15 This study focused on two time periods (26<sup>th</sup> – 31<sup>st</sup> July and 24<sup>th</sup> – 29<sup>th</sup> August, 2008) for application  
16 of the coupled hydrodynamic and temperature model. These periods were selected to avoid the  
17 complication of advected water and heat input from precipitation as identified by Brown and Hannah  
18 (2007) and Chikita et al. (2009). To characterize atmospheric conditions, meteorological variables were  
19 monitored using an Automatic Weather Station (AWS), which was located ~ 0.2 km from the snout of  
20 Kårsaglaciären and thus at the most westerly part of the study braidplain (Fig. 1). Air temperature and  
21 relative humidity were monitored using a Campbell CS215 probe. Incoming short-wave radiation was  
22 measured with a Skye Instruments SP1110 pyranometer. Wind speed and direction was measured using  
23 a RM Young 03002-5 CSL probe and stored on a Campbell CR200 datalogger.

24

25 < [Figure 2 near here](#) >

26

1 River stage was measured at 0.1 km and 5.4 km from the Kårsaglaciaren snout using Druck  
2 PDCR1830 pressure transducers interfaced with Campbell Scientific CR10X dataloggers. The  
3 instantaneous slug salt-dilution method was used to estimate discharge for flows ranging from 0.3 – 0.9  
4 m and a stage-discharge rating curve was constructed to yield discharge time-series. Water column  
5 temperature was monitored at 11 sites (Fig. 1C) along and across the braided river using Gemini  
6 Tinytag temperature dataloggers. At the river stage monitoring stations, water temperature was  
7 measured using Campbell Scientific CS547A temperature-electrical conductivity probes interfaced with  
8 Campbell CR10X dataloggers. All water temperature sensors were accurate to  $\pm 0.2^{\circ}\text{C}$ , cross-calibrated  
9 prior to field deployment, housed in radiation shields and logged values every 15 min. AWS and river  
10 stage sensors were scanned every 10 sec and averages stored every 15 min. All datalogger clocks were  
11 synchronised.

12

### 13 **Model domain specification**

14 An intensive high-resolution differential Global Positioning System (dGPS) field survey run in Real  
15 Time Kinematic (RTK) mode enabled collection of a network of topographic points in three-  
16 dimensional space (Fig. 1C). These points were then interpolated using an inverse distance weighting  
17 (IDW) algorithm to define a high-resolution (sub-meter) gridded Digital Elevation Model (DEM). This  
18 DEM comprised the braided channel network and overbank topography and served to delineate lateral,  
19 longitudinal and vertical properties of the computational field for the hydrodynamic model. This  
20 computational field was created via user-specified splines that enabled automatic generation of a  
21 curvilinear grid (Fig. 1C). This grid was refined in the lateral and longitudinal directions to create a  
22 mesh at  $\sim 1$  m resolution in horizontal space (Fig. 1C).

### 23 **Hydrodynamic model**

24

1 The hydrodynamic model used in this study is the open-source software Delft3D (WLDelft, 2010).  
2 Time-series of river discharge and water temperature (Fig. 2) were specified for upstream and  
3 downstream nodes (Fig. 1C). The model is forced to balance this upstream input and downstream output  
4 of water and thermal energy with additional exchange of thermal energy to/from the atmosphere.  
5 Several mesh nodes corresponding to field monitoring locations were ascribed as ‘history stations’ to  
6 extract modelled water temperature for assessment of model performance in space and time (Fig. 1C).

7  
8 Delft3D solves the Navier-Stokes equations for an incompressible fluid i) under the shallow water  
9 assumption in which vertical momentum is reduced to a hydrostatic pressure, and ii) with the  
10 Boussinesq assumption that momentum transfer caused by turbulent eddies can be modelled with an  
11 ‘eddy viscosity’. Governing laws of this model are described by the continuity and momentum  
12 equations, which are very well-known to be suitable for application to shallow river channels and  
13 braided river systems. They are fully documented within WLDelft (2010) and are not repeated here for  
14 brevity and because the focus of this paper is on the heat transport model. The model was run with a  
15 very short time step (0.001 mins.) and high spatial resolution; ~ 1 m mesh node spacing. We ran the  
16 hydrodynamic model with a single vertical layer; i.e. depth-averaged, and we considered that secondary  
17 circulation and sub-grid turbulence were negligible because of the high spatial resolution. Model bed  
18 elevation was fixed because field observations indicated that channel morphology remained unchanged  
19 during data collection. All model runs were primed with a 24-hour simulation of base flow ( $1 \text{ m}^3 \text{ s}^{-1}$ ) to  
20 ‘pre-wet’ the channel because this improved model performance of channel connectivity including  
21 hydraulic routing and diurnal expansion and contraction of the river channel network. Time integration  
22 of transport equations used an Alternating Direction Implicit (ADI) method, which is detailed in full by  
23 WLDelft (2010). However, due to the importance of the ADI for wetting and drying; i.e. for channel  
24 network expansion and contraction, such as that which occurs daily in proglacial braided river systems,  
25 we briefly summarise the method as follows. The first stage of the ADI method comprises the following  
26 four checks in the drying and flooding algorithm; i) drying check for velocity points in the longitudinal

1 direction, ii) drying check for velocity points in lateral direction and flooding check for velocity points  
2 in a lateral direction, iii) drying check for velocity points in a lateral direction during iterative solution  
3 for new water level, and iv) drying check (negative volumes) for water level points. In the second stage  
4 of the ADI method, directions are interchanged. Thus flow propagation, or ‘wetting’ was modelled as an  
5 advance of a kinematic wave over an initially dry bed and considered three factors; i) bed elevation at a  
6 water level point (cell centre), ii) water level at velocity point, and iii) criteria for ‘flooding’; i.e. setting  
7 a velocity and/or water level point to ‘wet’. Overall, this method means that flow propagation could  
8 only proceed by one mesh cell per model time-step. Furthermore, whether a mesh cell is deemed to be  
9 wet or not is determined by a user-specified threshold of the thickness of the wave boundary mixing  
10 layer, which was specified in this study as 0.1 m. For computational efficiency, meteorological and  
11 hydrological data were extracted at two hour intervals; cf. 15 minute resolution data acquisition in the  
12 field, for input to the hydrodynamic model.

13

## 14 **Heat transport model**

15

16 Water temperature was simulated using a heat transport model coupled to the hydrodynamic model.  
17 This heat transport model considers both vertical air-water interface energy exchanges and horizontal  
18 advective heat transfer due to fluid motion because these processes underpin hydraulics and thermal  
19 dynamics (Webb and Zhang, 1999; Hannah et al., 2004, Hannah et al., 2008). The heat transport model  
20 employs our direct field measurements of air temperature, relative humidity and incoming short-wave  
21 radiation. These variables are all considered to be globally uniform across the entire model domain and;  
22 thus, shading, sheltering and lapse-rates are not modelled. Energy balance terms not included are  
23 advective heat transport by precipitation and groundwater, and bed conduction and heat from fluid  
24 friction (cf. Hannah et al., 2004). Heat advection by groundwater (including hyporheic exchange) was  
25 not modelled because of i) the likely complex and high spatio-temporal variability of local ground-

1 surface water interactions (e.g. Malcolm et al., 2005) that could not be accurately quantified across the  
 2 relatively large study domain, and ii) uncertainties in estimating a reference temperature of  
 3 groundwater. Bed heat flux was not modelled because it has been reported to be a small component of  
 4 the overall river energy balance, particularly in summer (e.g. Webb & Zhang, 1997; Hannah et al., 2004,  
 5 2008). Bed friction is difficult to estimate accurately (Hannah et al., 2008) and indeed Moore et al.  
 6 (2005) omit a bed friction term altogether. We also simply assumed neutral atmospheric stability, which  
 7 is a common approach to avoid Richardson numbers etc.

8

9 The thermal capacity of a river depends on the water volume, with heat storage capacity increasing  
 10 and thus sensitivity to the energy budget decreasing as the water volume increases (Sinokrot and Stefan,  
 11 1993). Heat transfer from the atmosphere is driven by the change in water temperature  $T$  ( $^{\circ}\text{C}$ ) in the top  
 12 water ‘surface layer’ ‘ $S$ ’:

13

$$14 \quad \frac{\partial T_s}{\partial t} = \frac{Q_N}{\rho_w c_p \Delta z_s} \quad (1)$$

15

16 where  $Q_N$  ( $\text{J}\cdot\text{m}^{-2}\cdot\text{s}^{-1}$ ) is the total heat flux,  $c_p$  is the specific heat capacity of water ( $4181 \text{ J}\cdot\text{kg}^{-1}\cdot\text{C}^{-1}$ ),  $\rho_w$  is  
 17 the specific density of water ( $1000 \text{ kg}\cdot\text{m}^{-3}$ ) and  $\Delta z_s$  (m) is the water depth. The total heat flux was  
 18 specified as:

19

$$20 \quad Q_N = Q_A + Q_K + Q_L + Q_E + Q_H \quad (2)$$

21

22 where  $Q_N$  = net heat exchange ( $\text{J}\cdot\text{m}^{-2}\cdot\text{s}^{-1}$ ) as determined by both the horizontal advective heat flux  $Q_A$   
 23 ( $\text{J}\cdot\text{m}^{-2}\cdot\text{s}^{-1}$ ) and the vertical water surface energy balance terms, namely the surface shortwave solar  
 24 radiation flux  $Q_K$  ( $\text{J}\cdot\text{m}^{-2}\cdot\text{s}^{-1}$ ), surface net longwave radiation flux  $Q_L$  ( $\text{J}\cdot\text{m}^{-2}\cdot\text{s}^{-1}$ ), surface latent heat flux  $Q_E$

1 (J.m<sup>-2</sup>s<sup>-1</sup>) and the surface sensible heat flux  $Q_H$  (J.m<sup>-2</sup>s<sup>-1</sup>). Each of these heat flux components is detailed  
2 below.

3  
4 Advective heat transfer in rivers occurs primarily due to fluid motion. Thus we model advective heat  
5 flux  $Q_A$  by simply regarding heat as a quantity that is held within a mesh cell and passed to adjacent  
6 mesh cells. Advection of heat is determined in the model by the horizontal (fluid) velocity as modified  
7 by a horizontal diffusivity ( $D_v$ ). Advective velocity was calculated using the ADI scheme as briefly  
8 outlined above in the ‘hydrodynamic model’ section and  $D_v$  is determined by:

$$10 \quad D_v = \frac{u_c}{P} \quad (3)$$

11  
12 where  $u_c$  is user-specified horizontal eddy viscosity (0.01 m<sup>2</sup>s<sup>-1</sup>) and  $P$  is the dimensionless turbulence  
13 Prandtl-Schmidt number. A single value for eddy viscosity is appropriate for the whole model domain  
14 because the mesh cell size is near-uniform across the whole model domain and because flows are  
15 vertically well-mixed. Specification of a horizontal eddy viscosity (0.01 m<sup>2</sup>s<sup>-1</sup>) is essentially a  
16 consideration of turbulence because flows were shallow and vertically well-mixed. For such shallow  
17 water, it is assumed that the diffusion tensor is anisotropic; i.e. the horizontal eddy diffusivity far  
18 exceeds the vertical eddy diffusivity; 10 m<sup>2</sup>s<sup>-1</sup>.  $P$  approximates the ratio of momentum diffusivity  
19 (kinematic viscosity) and thermal diffusivity:

$$21 \quad P = \frac{c_p \cdot \mu}{k} \quad (4)$$

22  
23 where  $c_p$  = specific heat of water (4181 J.kg<sup>-1</sup>.°C<sup>-1</sup>),  $\mu$  = viscosity (Pa.s), and  $k$  = thermal conductivity  
24 (0.58 W.m<sup>-2</sup>°C<sup>-1</sup>).

25

1 Shortwave (solar) radiation  $Q_K$  at the water surface is assumed to be absorbed partially in the surface  
 2 layer  $S$  but ~50 % can be transmitted into the water column (e.g. Hannah et al., 2004). Specifically,  
 3 absorption of heat in the water column is an exponential function of the water depth:

$$4 \quad Q_K(z) = (1 - \xi)Q_K \frac{e^{-\gamma z}}{1 - e^{-\gamma H_{Turb}}} \quad (5)$$

6  
 7 where  $\xi$  (-) is the proportion of  $Q_K$  absorbed at the water surface, which is a function of the wavelength.  
 8 We use the Delft3d default value for  $\xi$  is 0.06 although we note that previously 0.4 has been suggested  
 9 (e.g. Edinger et al., 1968). The exact value of  $\xi$  does not matter too much because the water column  
 10 mixes rapidly and the total heat flux by short-wave radiation is distributed within the water column.  $z$  is  
 11 the water depth (m), and  $\gamma$  is the extinction coefficient ( $m^{-1}$ ) related to the turbidity ( $H_{Turb}$ ), which in the  
 12 model is given by proxy as a Secchi depth (m):

$$14 \quad \gamma = \frac{1.7}{H_{Turb}} \quad (6)$$

15  
 16 Net longwave radiation flux ( $Q_L$ ) is the balance between incoming longwave radiation  $Q_{L.in}$  and  
 17 emitted longwave radiation ( $Q_{L.out}$ ).  $Q_{L.in}$  was estimated from the Stefan-Boltmann's Law:

$$19 \quad Q_{L.in} = (1 - r)\varepsilon\sigma T_a^4 \quad (7)$$

20  
 21 where  $r$  is the albedo; reflection coefficient for water of 0.3,  $\varepsilon$  is an emissivity of 0.9 to consider the  
 22 generally turbid water and  $T_a$  ( $^{\circ}C$ ) is the air temperature.  $\varepsilon$  was modified between 0.7 for clear sky and  
 23 low temperature and 1.0 for cloudy sky and high temperature by relative humidity and air temperature  
 24 observations via the saturated vapour pressure  $e_w$  (mbar) and the actual vapour pressure  $e_a$  (mbar):

1

$$2 \quad e_w = 23.38e^{\frac{18.1 \cdot 53303.3}{T_a}} \quad (8)$$

3

$$4 \quad e_a = r_{hum} e_w \quad (9)$$

5

6 where  $r_{hum}$  is the relative humidity (%).

7

8  $Q_{L.out}$  from the water column was given by the Stefan-Boltzmann's Law (Oke, 1987), assuming a water  
 9 albedo; reflection coefficient, of 0.3 and an emissivity of 0.9 to consider the generally turbid water:

10

$$11 \quad Q_{L.out} = (1 - r)\epsilon\sigma T_s^4 \quad (10)$$

12

13 where  $\epsilon$  is an emissivity factor of 0.985 for water,  $T_s$  is the absolute water temperature (K).

14

15 Latent heat ( $Q_E$ ) lost by evaporation or gained by condensation ( $E_v =$  evaporation/condensation rate,  
 16  $\text{mm}^{\text{d}^{-1}}$ ) was estimated by:

17

$$18 \quad Q_E = L_v \rho E_v \quad (11)$$

19

20 where  $\rho$  is the specific weight of water ( $1000 \text{ kg.m}^{-3}$ ) and  $L_v$  is the latent heat of vaporisation ( $\text{J.kg}^{-1}$ )  
 21 given by:

22

$$23 \quad L_v = 2.5 \times 10^6 - 2.3 \times 10^3 T_a \quad (12)$$

24

1 where  $T_a$  ( $^{\circ}\text{C}$ ) is air temperature (e.g. Webb and Zhang, 1999). The evaporation rate  $E_v$  defined as the  
2 volume of water evaporated per unit area per unit time is computed using Dalton's law of mass transfer:

$$3 \quad E_v = fU_2(e_s - e_a) \quad (13)$$

4  
5  
6 where  $fU_2$  is the Dalton number of 0.0012 multiplied by the average wind speed at 2 m above the  
7 surface and where  $e_w$  and  $e_a$  are as given in equations 8 and 9, respectively.

8  
9 Sensible heat transfer  $Q_H$  was estimated as the product of the Bowen ratio (Bowen, 1926) and the  
10 latent heat flux:

$$11 \quad Q_H = R_b Q_E \quad (14)$$

$$12 \quad R_b = \beta \frac{(T_s - T_a)}{(e_w - e_a)} \quad (15)$$

13  
14  
15  
16 with  $\beta$  (-) = Bowen constant (0.61).

## 17 18 **Model sensitivity**

19  
20 The sensitivity of modelled water temperature to selected parameters, excluding meteorological  
21 forcing, was assessed by a series of individual modelling experiments to isolate the influence of each  
22 parameter. For brevity, only results from one main channel site (Z07) and factors with high water  
23 temperature sensitivity are presented, namely turbidity (Fig. 3A), horizontal eddy diffusivity (Fig. 3B),  
24 and downstream boundary water temperature (Fig. 3C). Turbidity and downstream boundary water

1 temperature displayed logarithmic relationships with the mean deviation of modelled water temperature  
2 from measured water temperature (Figs. 3D and 3F), whilst horizontal eddy diffusivity had an inverse  
3 linear relationship (Fig. 3E). However, turbidity had a negligible effect on modelled water temperature  
4 (Fig. 3A) because the majority of the model domain has shallow water depth. Water temperature at the  
5 downstream boundary node had the largest influence (Fig. 3C) and produces a forcing that propagated  
6 upstream as the model equilibrates. This forcing initially surprised us but we realise that in reality it is  
7 due to interactions of lake water with near-stagnant deltaic streams. In the model this upstream forcing  
8 effect occurred between ‘Main 7’ and the downstream Boundary node (Fig. 1) and thus outside of our  
9 area of interest, which is on the uppermost (westernmost) reach; the braidplain.

10

## 11 **Model performance**

12

13 Model performance was evaluated quantitatively using a number of goodness of fit statistics (Table 1)  
14 as described and used by Hannah and Gurnell (2001) which assessed absolute numerical agreement, and  
15 similarity of form with time. Overall, model performance decreased as the range of water temperature at  
16 a site increased. During both time periods, it is clear that the model accurately replicated the shape,  
17 timing and magnitude of the diurnal river thermograph at a representative main channel site (Fig. 4A, D;  
18 Table 1). However, at sites in the centre of the braidplain in Period 1 the model tended to underestimate  
19 observations (Table 1), generated some unobserved oscillations, and lagged behind the timing of the  
20 daily peak water temperature by 1 – 1.5 hours (Fig. 4B). This lag was most pronounced for sites at the  
21 lateral margins of the braidplain. Similarly, during Period 2 at this mid-braidplain site, the model did not  
22 accurately represent the timing of the daily peak water temperature (Table 1; Fig. 4E). At the marginal  
23 site, the modelled timing of peak water temperature was accurate, yet maximum and minimum water  
24 temperature was overestimated and underestimated (respectively) by  $\sim 3^{\circ}\text{C}$  in the first time period (Fig.  
25 4C) and by  $> 4^{\circ}\text{C}$  during the second time period (Fig. 3F).

1  
2  
3  
4  
5  
6  
7  
8  
9  
10  
11  
12  
13  
14  
15  
16  
17  
18  
19  
20  
21  
22  
23  
24  
25

< Figure 4 near here >

< Table 1 near here >

## Quantifying spatio-temporal variability in water temperature

The hydrodynamic model offered the opportunity to examine temporal variability; specifically thermal connectivity and spatio-temporal thermal heterogeneity, in water temperature across the entire wetted area of the model domain (Figure 5). A novel analysis of the temporal variability of water temperature across the entire model domain was achieved by exporting model grids at one hour intervals to ascii format, and running a bespoke Java code (Turner, 2010) to produce a histogram, descriptive statistics and heterogeneity indices for each of these model grids. Thus a time-series of water temperature variability across the entire model domain was produced by this analysis of one-hour interval model grid outputs. Modelled water temperature had a histogram constructed from ~90,000 modelled (grid cell) values whilst the measured water temperature histogram comprised data from just 11 measured sites in the field. Thus, we calculated the hourly value of three higher-order spatial heterogeneity indices, namely dominance, diversity and evenness/equitability (e.g. Turner, 1990; Bower et al., 2004) to enable a comparison between modelled and measured water temperatures.

From spatially-gridded model output at hourly increments, we firstly computed the mean water temperature per mesh cell, which for the vast majority of the system was 0.5 – 2.0 °C (Fig. 5A). During Period 1, the minimum water temperature across the entire wetted area, which expanded and contracted diurnally in response to dynamic meltwater inputs from glacier- and snow-melt, was relatively uniform at 1 – 2 °C (Fig. 5B). There was shallow water (< 0.1 m) and flow stagnation where the model simulated very high water temperature (Figure 5B). The maximum water temperature was much more spatially

1 variable compared to minimum water temperature, with main channel zones  $< 4^{\circ}\text{C}$  and channels  
2 marginal to the braidplain reaching  $> 12\text{-}14^{\circ}\text{C}$  (Table 1; Fig. 5C). Given this variability, we obtained the  
3 modelled range of water temperature as a proxy statistic for the water temperature regime (Fig. 5D).

4

5 [< Figure 5 near here >](#)

6

7 The modelling in this project enables visualisation and quantitative analysis of the connectivity and  
8 thermal heterogeneity of the whole river system, in comparison to only relatively few single site water  
9 temperature measurements (Fig. 6). Specifically, the most salient feature is a clear diurnal cycle where  
10 water temperatures not only increase towards early afternoon but also become more 'diverse' in space  
11 (Fig. 6). While hourly mean values were not greatly different between the model and the field  
12 measurements for either time period, standard deviation was considerably different (Fig. 6A). Hourly  
13 modelled standard deviations were both of a greater magnitude and also had larger daily amplitude than  
14 standard deviations of hourly measured water temperatures (Fig. 6A).

15

16 The transient nature of thermal heterogeneity across the braidplain was further evident from grid-  
17 based analysis of modelled water temperatures. Measured and modelled skewness and kurtosis values  
18 calculated for hourly grids of water temperature were generally in disagreement with each other in  
19 direction, magnitude and temporal phase (Fig. 6B). This is a clear indication that the spatial distribution  
20 of water temperatures across the modelled domain had a greater temporal heterogeneity than was  
21 recorded by dataloggers at the eleven field measurement sites. These indices also showed diurnal cycles  
22 (Fig. 7) illustrating the increase and decrease of thermal heterogeneity during the diurnal cycle.  
23 However, the diversity index was not as sensitive as the dominance index (Fig. 7), because it is  
24 calculated as the deviation from the maximum possible diversity at a given scale; i.e. in this case model  
25 cell size (Turner, 1990).

26

1 < Figure 6 near here >

2

3 < Figure 7 near here >

## 4 **Discussion**

5

6 This study has illustrated the potential utility of combining high-resolution digital elevation models,  
7 direct measurements of river water temperature at spatially discrete sites, meteorological observations  
8 and river hydrodynamic and heat transport models to understand spatio-temporal water column thermal  
9 heterogeneity. The thermal dynamics identified herein could not have been observed with air - water  
10 temperature regression (e.g. Loheide and Gorelick, 2006; Cardenas, 2009) and stochastic methods  
11 (Caissie, 2006; Webb et al., 2008) because these common approaches are zero-dimensional and seek to  
12 simulate single-site measurements. Deterministic modelling has hitherto usually been carried out as a  
13 one-dimensional problem (Caissie, 2006) where temperature is simulated either along the principal  
14 longitudinal axis of a river, or at-a-point over a period of time (e.g. Chikita et al., 2009). This follows a  
15 commonly-held assertion that water temperature is relatively uniform with depth and that only small  
16 changes are observed in the lateral direction (i.e. that rivers are well-mixed cf. Clark et al., 1999). This  
17 may be the case for some hydraulically rough, single-thread stable channels without multiple water  
18 sources. However, our study illustrates i) persistent thermal patterns between the main river channel and  
19 side channels, and ii) particularly strong lateral variability in water temperature.

20

21 The hydrodynamic model simulated water temperature well in space and time when at-a-point  
22 predictions were extracted for comparison with the observed water temperature records. For example  
23 *RMSE* for the main channel (0.3 - 2.4°C) and for sites on the lateral margins of the river network (0.6 -  
24 3.8°C) are similar to the range of error obtained from other deterministic modelling studies that were  
25 focused relatively on single-site temporal changes or longitudinal changes (Marceau et al., 1986: 1.4 -

1 2.9 °C; Sinokrot and Stefan, 1993: < 1.1 °C; Younus et al., 2000: 1.3 °C; Caissie et al., 1998: 0.6 - 1.7  
2 °C; Caissie et al., 2005: 1.1 - 1.5 °C). With some knowledge of the field conditions, it can be stated that  
3 the variable 'range of water temperature' (Fig. 5D) discriminates very clearly between water sources.  
4 Specifically, it is possible to identify i) streams that are almost entirely glacier-fed (range 0.5 – 2.0 °C;  
5 Table 1; Fig. 5D), ii) streams that intermittently receive fluctuating water source contributions, and; iii)  
6 streams at the lateral margin of the braidplain that are characterized by very high thermal heterogeneity  
7 (range > 8 °C; Table 1; Fig. 5D).

8  
9 The novel application of our heat transport model albeit with its inherent limitations serves as a tool to  
10 infer dominant controls on water temperature in space and through time. The good model performance  
11 in the main channel suggests that bed conduction heat fluxes; i.e. frictional, groundwater and hyporheic  
12 heat sources/sinks, are negligible for stable channels with persistent longitudinal connectivity. This  
13 negligible influence of bed heat flux for river channels is in agreement with the findings of Webb and  
14 Zhang (1997) and Hannah et al. (2004, 2008) for a temperate environment and and alpine environments,  
15 respectively, but in disagreement with the suggestions of Story et al. (2003) and Cozzetto, McKnight et  
16 al. (2006), which are studies in a temperate and polar environment, respectively. Prediction of thermal  
17 oscillations for sites in the centre of the braidplain was not observed in the field. These oscillations  
18 could be due to i) a modelled change in water source contributions and water (initial) temperature (cf.  
19 Cadbury et al., 2008), ii) insufficient 'buffering' in the model of the instantaneous radiative flux, or iii)  
20 an antecedent control of the temperature of the gravel bars prior to becoming inundated, or 'wetted' by  
21 the model during episodes of flow network expansion (c.f. Burkholder et al., 2008; Cardenas, 2010).  
22 Additionally, we suggest that some high-frequency variability was not dampened because of a small  
23 thermal capacity limit (i.e. mesh cells size) and due to shallow water depths.

24  
25 In explanation of the relatively poor performance of the model for marginal channel sites, it is  
26 important to note that marginal channels are ephemeral as controlled by channel network changes; i.e.

1 diurnal braidplain expansions and contractions. Our modelling of this ephemeral character may need to  
2 be modified for several reasons. Firstly, the hydraulic treatment of mesh cell wetting and drying  
3 assumes that a mesh cell is dry if zero velocity persists with a minimum water depth of 0.1 m. Secondly,  
4 our model specifies meteorological conditions ‘globally’ (i.e. uniformly over the whole model domain).  
5 This discretization is erroneous because topographic shading could be important at marginal channel  
6 sites. Thirdly, our modelling hints that ground heat flux can be an important driver of water temperature  
7 where water is shallow and slow-moving or stagnant, where exchange of heat from groundwater and  
8 hyporheic sources is pronounced (Hannah *et al.*, 2009) and/or where-hillslope processes are prevalent  
9 (e.g. Loheide and Gorelick, 2006). Fourthly we only measured water temperature and not water depth or  
10 flow velocity at braidplain sites (Z01 – Z13) and so cannot be sure of the degree to which the wetting  
11 and drying evident in the model is accurate.

12

13 There is some evidence that the performance of the model also depends on prevailing weather  
14 conditions. Model simulations of water temperature were less robust for Period 2. This period was  
15 characterized by a lower net radiative flux than Period 1 (Fig. 2D) when there was far more cloud cover.  
16 The inference is that radiation is the dominant heat transfer process and that the other heat fluxes were  
17 not so well modelled. There is clearly a need for future comparison of energy budget schemes to  
18 determine the relative importance (and model performance) of heat flux components. Additionally, we  
19 purposefully chose not to model days with rainfall because these heat transfers have to be explicitly  
20 measured and quantified before being written into a numerical model. We only possess summer field  
21 data on water temperatures. Therefore, further research is required to assess model performance across  
22 other temperature ranges or extremes and seasons.

23

24 Our modelling shows that spatio-temporal calculations of water temperature are crucial to consider  
25 the interaction of three key parts of deterministic models, particularly in systems with ephemeral and  
26 multi-scale components. These three parts are process-representations determined per mesh cell herein

1 and include: i) heat energy imported and exported, ii) thermal capacity exposed to that energy, and iii)  
2 antecedent water temperature raised/lowered by that heat exchange. The issues encountered in this study  
3 with modelling these three sets of processes are most evident in our sensitivity analyses, which show the  
4 dominance of the advective processes over dispersion in relatively shallow and fast-moving water, and  
5 in the fact that marginal channels are relatively poorly simulated. Channels at the lateral margin of the  
6 braidplain have very high width-depth ratios, a very small volume and consequently a large modelled  
7 thermal range. In addition, it is probable that marginal sites receive hydrological inputs from hillslopes  
8 and springs that will advect more thermally stable waters (Brown and Hannah, 2007); these  
9 hydrological fluxes are beyond representation in the current modelling scheme. Further investigation is  
10 required to determine if this reduced predictability is indicative of issues with either the water volume;  
11 i.e. thermal capacity, flow rate, hydraulic retention and time for equilibration. Alternatively, there may  
12 be a limit to the advection-dispersion performance linked to the size of the computational mesh because  
13 some river channels are narrower/shallower than the mesh resolution. This highlights the importance of  
14 accurate and high resolution DEMs of channel bathymetry and overbank topography as well as  
15 (computationally efficient) high resolution model meshes.

16

17 This study indicates the potential for deterministic models to represent thermal connectivity and  
18 spatio-temporal thermal heterogeneity in rivers with multiple channels and/or with significant lateral  
19 variability. A major benefit of deterministic models of water temperature is the potential to develop  
20 insights into spatio-temporal thermal heterogeneity, something that is not possible from sparse at-a-  
21 point field measurements. Thus, in contrast to previous studies focussing on the thermal ‘heterogeneity’  
22 of river systems (e.g. Brown and Hannah, 2001; Arscott et al., 2001; Tonolla et al., 2010) we were able  
23 for the first time to highlight and quantify the coherence/complexity and robustness/sensitivity of patch-  
24 scale river water temperature distribution with both magnitude and temporal fluctuations. This  
25 emphasises that quantification of thermal heterogeneity is not straightforward and depends both on the  
26 scale and on the statistical approach adopted. For example, whilst the diversity, dominance and

1 evenness indices all followed a clear and relatively smooth diurnal cycle (Fig. 7), evenness was notably  
2 more variable. This is because the evenness index responds to the probability that a pixel belongs to a  
3 patch type, and to the number of patch types and their proportions in a landscape. In this case, a patch is  
4 a group of grid cells with water temperature belonging to a 0.25 °C interval of the histogram. Evenness  
5 is thus a surrogate for not only the magnitude of spatial heterogeneity but it also appears to indicate the  
6 rate of change of that heterogeneity. Overall, with development this approach could be used to identify  
7 thermal pulses linked to the wetting and drying, and thus heating and cooling, of parts of the river  
8 system as individual channels activate and stagnate with avulsions and river network changes. However,  
9 on the basis of the investigations in this study, we consider that should such significant channel  
10 avulsions or network changes occur, for instance river expansion laterally overbank or across valley  
11 floors, knowledge of the antecedent ground temperature and thermal characteristics of the ground would  
12 be important for determining water temperature. Thus a land cover model and a land surface heat budget  
13 model would be required, as well as a hydrodynamic-heat transport model.

14  
15 More widely, it is clear that further development of deterministic models could be especially suitable  
16 for applications such as analyzing sensitivity to environmental change through scenario-based  
17 manipulations (Caissie et al., 2005). In the case of the Arctic, hydrological change will be dependent on  
18 a changing climate (Lammers et al., 2007) and as our modelling suggests most notably by changes in  
19 the radiation balance. Models should thus examine the effect of river discharge magnitude and timing  
20 and changing surface energy balance on water temperature. Other reach-based studies that would benefit  
21 from scenario-based two-dimensional modelling include those producing management plans to examine  
22 the interplay between climate, hydrology and geomorphology in situations where rivers are affected by  
23 riparian modification (Mitchell, 1999), or those quantifying river rehabilitation or restoration works (e.g.  
24 Horne et al., 2004; Null et al., 2009). In such circumstances, a spatio-temporal representation of the  
25 river thermal regime would enable testing of various scenarios to find solutions to produce thermal  
26 heterogeneity commensurate with any ecological aims of a given restoration scheme.

1

## 2 **Conclusions**

3

4 This study presents the governing equations and method for coupling a heat transport model to a two-  
5 dimensional hydrodynamics model. It tests this method with a high-resolution hydrodynamic model and  
6 evaluates this approach for interpolating spatial and temporal at-a-point measurements of water  
7 temperature. In a comparison of distributed water temperature model predictions with field observations  
8 it demonstrates how water temperature can be numerically modelled through time over two-dimensional  
9 space, and analyzed to discriminate thermal regimes dependent on longitudinal and lateral river  
10 hydrodynamics. This has been achieved by exploiting the benefits of recent technological advances in  
11 digital surveying, automatic environmental sensors and hydrodynamic modelling.

12

13 Model goodness of fit statistics yield  $r$  values  $> 0.9$ ,  $RMSEs \sim 0.6$  °C and  $ME < 0.4$  °C for main  
14 channels. However, model performance decreased for sites characterized by shallow and/or temporarily-  
15 stagnant water at the lateral margins of the braidplain. A lag of 60 – 90 mins. persisted between the  
16 modelled and measured water temperature for sites on the lateral margin of the braidplain. As a method  
17 for interpolating between multi-site observations, our model reveals flow pulses linked to the wetting  
18 and drying of the system as individual channels activate and stagnate with avulsions and river network  
19 changes, and shows how these are superimposed upon the diurnal thermal cycle. Future numerical  
20 modelling efforts should aim to develop the sensitivity analyses of this study into a full discrimination  
21 of the contributions of major heat flux components. In this manner, an understanding of fundamental  
22 energy transfer processes will aid model transferability to wider applications. Spatially-varied  
23 meteorological conditions should be considered to accommodate shading and sites with local  
24 microclimates due to topographic or riparian shading, for example. Future modelling will benefit from  
25 utilizing not only field-deployed array of sensors, as in this study, but also infra-red cameras (Torgerson

1 et al., 2001; Tonolla et al., 2010) that can yield calibration and validation data with spatial and temporal  
2 coverage akin to that of the model domain. Such scenario-based modelling and future projection of  
3 hydrological patterns and hydraulic conditions would also be of value in other studies, such as finding  
4 optimal solutions for river remediation (e.g. Hester and Gooseff, 2010) where changes in channel  
5 morphology or flow are likely to drive alterations to the thermal regime, or within studies concerned  
6 with heated effluent discharges.

7

## 8 **Acknowledgements**

9

10 JLC, LEB and DMH were in receipt of Transnational Access Programme (ATANS) FP6 506004  
11 grants awarded through the Abisko Scientific Research Station. JLC and LEB were also supported by  
12 the Royal Geographical Society H.R. Mill Trust Fund (GFG 08/07) and by a School of Geography  
13 (Leeds) research development fund grant. Katherine Arrell, David Ashley, Christopher Mellor,  
14 Alexander Milner and Clare Plant provided much appreciated assistance in the field.

15

16

17

## References

- Arscott, D.B., Tockner, K., Ward, J.V., 2001. Thermal heterogeneity along a braided floodplain river (Tagliamento River, northeastern Italy). *Canadian Journal of Fisheries and Aquatic Sciences* 58, 2359-2373.
- Bowen, I.S., 1926. The ratio of heat losses by conduction and evaporation from any water surface. *Phys. Rev.* 27, 779–787.
- Bower, D., Hannah, D.M., McGregor, G.R., 2004. Techniques for assessing the climatic sensitivity of river flow regimes. *Hydrological Processes* 18, 2515–2543.
- Brown, L.E., Hannah, D.M., Milner, A.M., 2007. Vulnerability of alpine stream biodiversity to shrinking glaciers and snowpacks. *Global Change Biology* 13, 958-966.
- Brown, L.E., Hannah D.M., 2007. Alpine stream temperature response to storm events. *Journal of Hydrometeorology* 8, 952-967.
- Brown, L.E., Hannah, D.M., 2008. Spatial heterogeneity of water temperature across an alpine river basin. *Hydrological Processes* 22, 954-967.
- Burkholder, B.K., Grant, G.E., Haggerty, R., Khangaonkar, T., Wampler, P.J., 2008. Influence of hyporheic flow and geomorphology on temperature of a large, gravel-bed river, Clackamas River, Oregon, USA. *Hydrological Processes* 22, 941–953
- Caissie, D., 2006. The thermal regime of rivers: a review. *Freshwater Biology* 51, 1389-1406.
- Caissie, D., Satish, M.G., El-Jabi, N., 2005. Predicting river water temperatures using the equilibrium temperature concept with application on Miramichi River catchments (New Brunswick, Canada). *Hydrological Processes* 19, 2137-2159.
- Caissie, D., El-Jabi, N., St-Hilaire, A., 1998. Stochastic modelling of water temperatures in a small stream using air to water relations. *Canadian Journal of Civil Engineering* 25, 250–260.
- Cardenas, M.B., 2010. Lessons from and assessment of Boussinesq aquifer modeling of a large fluvial island in a dam-regulated river. *Advances in Water Resources* 33, 1359-1366.
- Cardenas, M.B., 2009. Stream-aquifer interactions and hyporheic exchange in gaining and losing sinuous streams. *Water Resources Research* 45, W06429.
- Cardenas, M.B., Harvey, J.W., Packman, A.I., Scott, D.T., 2005. Ground-based thermography of fluvial systems at low and high discharge reveals complex thermal heterogeneity driven by flow variation and bioroughness, *Hydrological Processes* 22, 980-986
- Chikita, K. A., Kaminaga, R., Kudo, I., Tomoyuki, W., Yongwon, K., 2009. Parameters determining water temperature of a proglacial stream: the Phelan creek and the Gulkana glacier, Alaska. *River Research and Applications* 26, 995–1004
- Clark, E., Webb, B.W., Ladle, M., 1999. Microthermal gradients and ecological implications in Dorset rivers. *Hydrological Processes* 13, 423–438.
- Cozzetto, K., McKnight, D., Nylen T., Fountain, A., 2006. Experimental investigations into processes controlling stream and hyporheic temperatures, Fryxell Basin, Antarctica. *Advances in Water Resouces* 29, 130-153.
- Durance, I., Ormerod, S.J., 2007. Climate change effects on upland stream macroinvertebrates over a 25-year period. *Global Change Biology* 13, 942-957.
- Edinger, J.E., Duttweiler, D.W. and Brady, R. 1968. The response of water temperature to meteorological conditions, *Water Resources Research* 4, 1137-1145.
- Hannah D.M., Malcolm I.A. and Bradley C. 2009, Seasonal hyporheic temperature dynamics over riffle bedforms, *Hydrological Processes* 23, 2178-2194.
- Hannah, D.M., Gurnell, A.M., 2001. A conceptual, linear reservoir runoff model to investigate melt season changes in cirque glacier hydrology. *Journal of Hydrology* 246, 123-141.

- 1 Hannah, D.M., Malcolm, I.A., Soulsby, C., Youngson, A.F., 2004. Heat exchanges and temperatures  
2 within a salmon spawning stream in the Cairngorms, Scotland: Seasonal and sub-seasonal  
3 dynamics. *Rivers Res. Apps.* 20, 635-652.
- 4 Hannah, D.M., Brown, L.E., Milner, A.M., Gurnell, A.M., McGregor, G.R., Petts, G.E., Smith B.P.G.,  
5 Snook, D.L., 2007. Integrating climate-hydrology-ecology for alpine river systems. *Aquatic  
6 Conservation: Marine and Freshwater Ecosystems* 17, 636–656.
- 7 Hannah, D.M., Malcolm, I.A., Soulsby, C., Youngson, A.F., 2008. A comparison of forest and  
8 moorland stream microclimate, heat exchanges and thermal dynamics. *Hydrological Processes*  
9 22, 919-940.
- 10 Hannah, D.M., Malcolm, I.A., Bradley, C., 2009. Seasonal hyporheic temperature dynamics over riffle  
11 bedforms. *Hydrological Processes* 23, 2178-2194.
- 12 Hawkins, C.P., Hogue, J.N., Decker, L.M., Feminella, J.W., 1997. Channel morphology, water  
13 temperature, and assemblage structure of stream insects. *Journal of the North American  
14 Benthological Society* 16: 728-749.
- 15 Hester, E.T., Gooseff, M.N., 2010. Moving beyond the banks: Hyporheic restoration is fundamental to  
16 restoring ecological services and functions of streams. *Environ. Sci. Technol.* 44 (5), 1521-1525.
- 17 Horne, B.D., Rutherford, E.S., Wehrly, K.E., 2004. Simulating effects of hydro-dam alteration on  
18 thermal regime and wild steelhead recruitment in a stable-flow Lake Michigan tributary. *Rivers  
19 Res. Apps.* 20, 185-203.
- 20 Lammers, R.B., Pundsack, J.W., Shiklomanov, A.I., 2007. Variability in river temperature, discharge  
21 and energy flux from the Russian pan-Arctic landmass. *Journal of Geophysical Research* 112,  
22 G04S59.
- 23 Habin Li, H., Reynolds, J.F., 1994. A simulation experiment to quantify spatial heterogeneity in  
24 categorical maps. *Ecology* 75, 2446-2455.
- 25 Lammers, R.B., Pundsack, J.W., Shiklomanov, A.I., 2007. Variability in river temperature, discharge,  
26 and energy flux from the Russian pan-Arctic landmass. *Journal of Geophysical Research -  
27 Biogeosciences* 112 (G4): G04S59.
- 28 Loheide, S.P., Gorelick, S.M., 2006. Quantifying stream-aquifer interactions through the analysis of  
29 remotely sensed thermographic profiles and in situ temperature histories. *Environ. Sci. Technol.*  
30 40, 3336-3341.
- 31 Marceau, P., Cluis, D., Morin, G., 1986. Comparaison des performances relatives à un modèle  
32 déterministe et à un modèle stochastique de température de l'eau en rivière. *Canadian Journal of  
33 Civil Engineering* 13, 352 - 364.
- 34 Milner, A.M., Brown, L.E., Hannah, D.M., 2009. Hydroecological response of river systems to  
35 shrinking glaciers. *Hydrological Processes* 23, 62-77.
- 36 Mitchell, S., 1999. A simple model for estimating mean monthly stream temperatures after riparian  
37 canopy removal. *Environmental Management* 24, 77-83.
- 38 Null, S.E., Deas, M.L., Lund, J.R., 2009. Flow and water temperature simulation for habitat restoration  
39 in the Shasta River, California. *River Research and Applications* 26, 663–681.
- 40 Octavia, K.A.H., Jirka, G.H., Harleman D.R.F., 1977. Vertical heat transport mechanisms in lakes and  
41 reservoirs. Massachusetts Institute of Technology, Report no 227.
- 42 Oke, T.R. 1987. *Boundary layer climates*, 2nd edition, Methuen, London.
- 43 Schiermeier, Q., 2006. On thin ice. *Nature* 441, 147-148.
- 44 Sinokrot, B.A., Stefan, H.G. 1993. Stream temperature dynamics - measurements and modelling. *Water  
45 Resources Research* 29, 2299-2312.
- 46 Story A., Moore R.D., Macdonald J.S., 2003. Stream temperatures in two shaded reaches below  
47 cutblocks and logging roads: downstream cooling linked to subsurface hydrology. *Canadian  
48 Journal of Forest Research* 33, 1383-1396.
- 49 Streeter, V.L.; Wylie, E.B., 1981. *Fluid mechanics*, McGraw-Hill.
- 50 Tonolla, D., Vicenc, Acuna, V., Uehlinger, U., Frank, T., Tockner, K., 2010. Thermal Heterogeneity in  
51 River Floodplains. *Ecosystems* 13, 727–740.

- 1 Torgersen, C.E., Faux, R.N., McIntosh, B.A., Poage, N.J., Norton, D.J., 2001. Airborne thermal remote  
2 sensing for water temperature assessment in rivers and streams. *Remote Sensing of Environment*  
3 76, 386–398.
- 4 Turner, A.G., 2010. Stream Temperature Grid Generalisation Source Code Web Page.  
5 [http://www.geog.leeds.ac.uk/people/a.turner/src/andyt/java/projects/StreamTemperatureGridGen](http://www.geog.leeds.ac.uk/people/a.turner/src/andyt/java/projects/StreamTemperatureGridGeneralisation/)  
6 [eralisation/](http://www.geog.leeds.ac.uk/people/a.turner/src/andyt/java/projects/StreamTemperatureGridGeneralisation/) last accessed 10/11/2010
- 7 Turner, M.G., 1990. Spatial and temporal analysis of landscape patterns. *Landscape Ecology* 4, 21-30.
- 8 Webb, B.W., Zhang, Y., 1999. Water temperatures and heat budgets in Dorset chalk water courses.  
9 *Hydrological Processes* 13, 309-321.
- 10 Webb, B.W., Hannah, D.M., Moore, R.D., Brown, L.E.; Nobilis, F., 2008. Recent advances in stream  
11 and river temperature research. *Hydrological Processes* 22, 902-918.
- 12 WLDelft., 2010 Delft3D user and technical support manuals. <http://delftsoftware.wldelft.nl> Last  
13 accessed 30th September 2010.
- 14 Younus, Y., Hondzo, M., Engel, B.A., 2000. Stream temperature dynamics in upland agricultural  
15 watersheds. *Journal of Environmental Engineering-ASCE* 126, 518–526.
- 16 Young, R.G., Collier K.J., 2009. Contrasting responses to catchment modification among a range of  
17 functional and structural indicators of river ecosystem health. *Freshwater Biology* 54, 2155-  
18 2170.
- 19

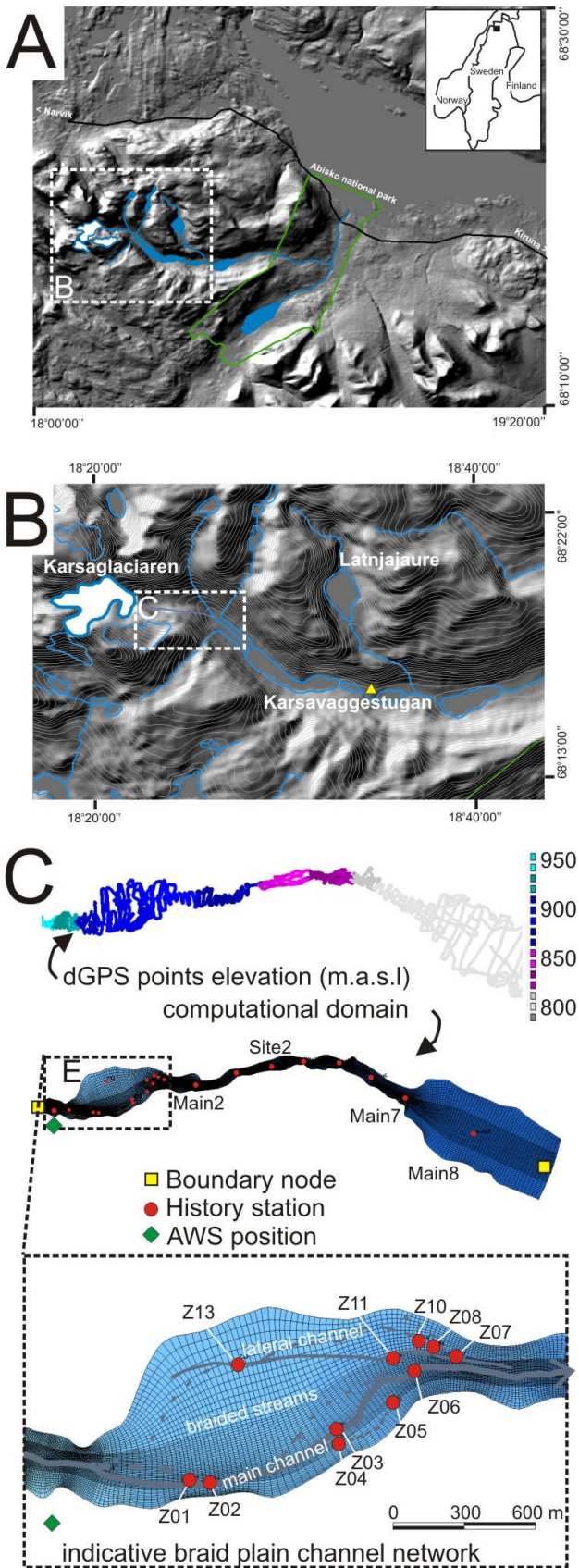
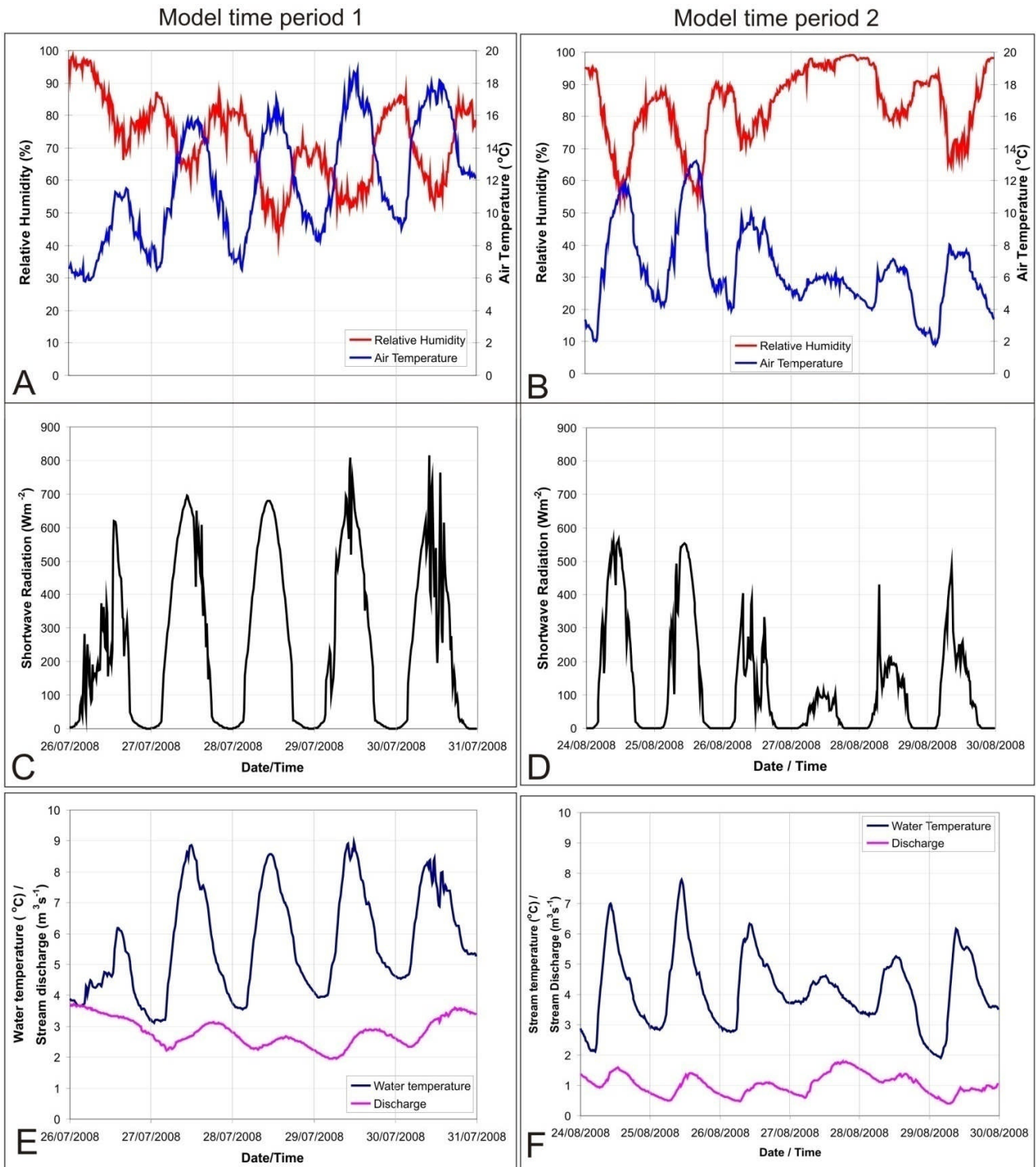


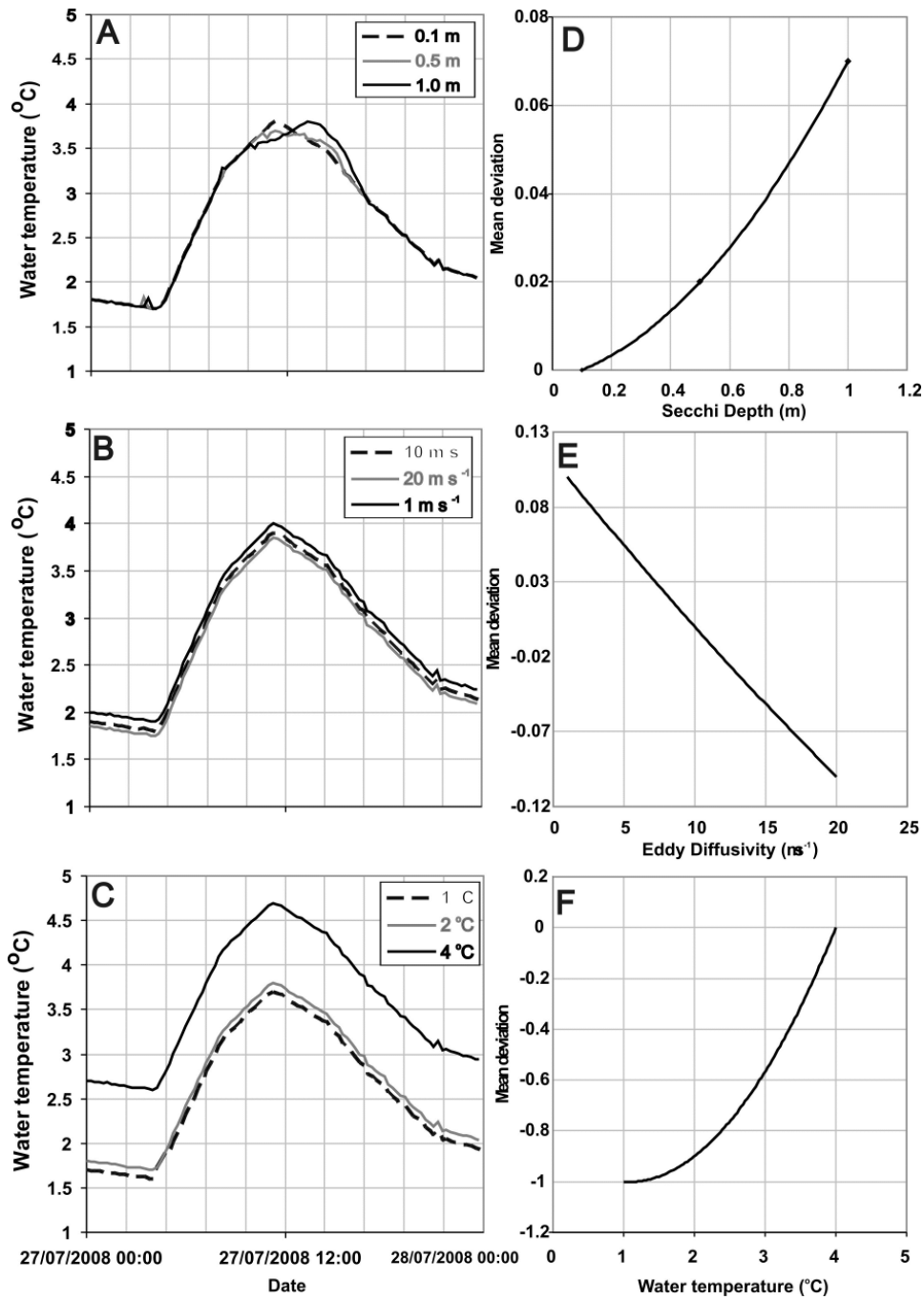
**Figure 1.** The Kårsajokk River in Arctic Sweden (A) is predominantly fed from Kårsaglaciaren and comprises both single-thread and braided sections (B). High-resolution topography was gained via interpolation from an intensive dGPS RTK survey (C). This survey delimited the model domain, across which a computational mesh was constructed and refined to ~ 1 m horizontal resolution (C). Topography was mapped onto this mesh, and time-series data (Fig. 2) specified for the upstream and downstream boundary nodes. Modelled hydraulics and water temperature were computed in continuous space and at hourly time intervals and additionally at eleven sites Z01 – Z13 where field measurements were made. Note that Z09 and Z12 do not exist.



1

2

3 **Figure 2.** Time-series data input to stream temperature model. Automatic Weather Station (AWS)  
 4 records for air temperature and relative humidity (A, B) and incoming shortwave radiation (C, D) were  
 5 specified uniformly across the entire model domain. In each time period the upstream boundary was  
 6 specified for time-varying stream discharge and water temperature (E, F).

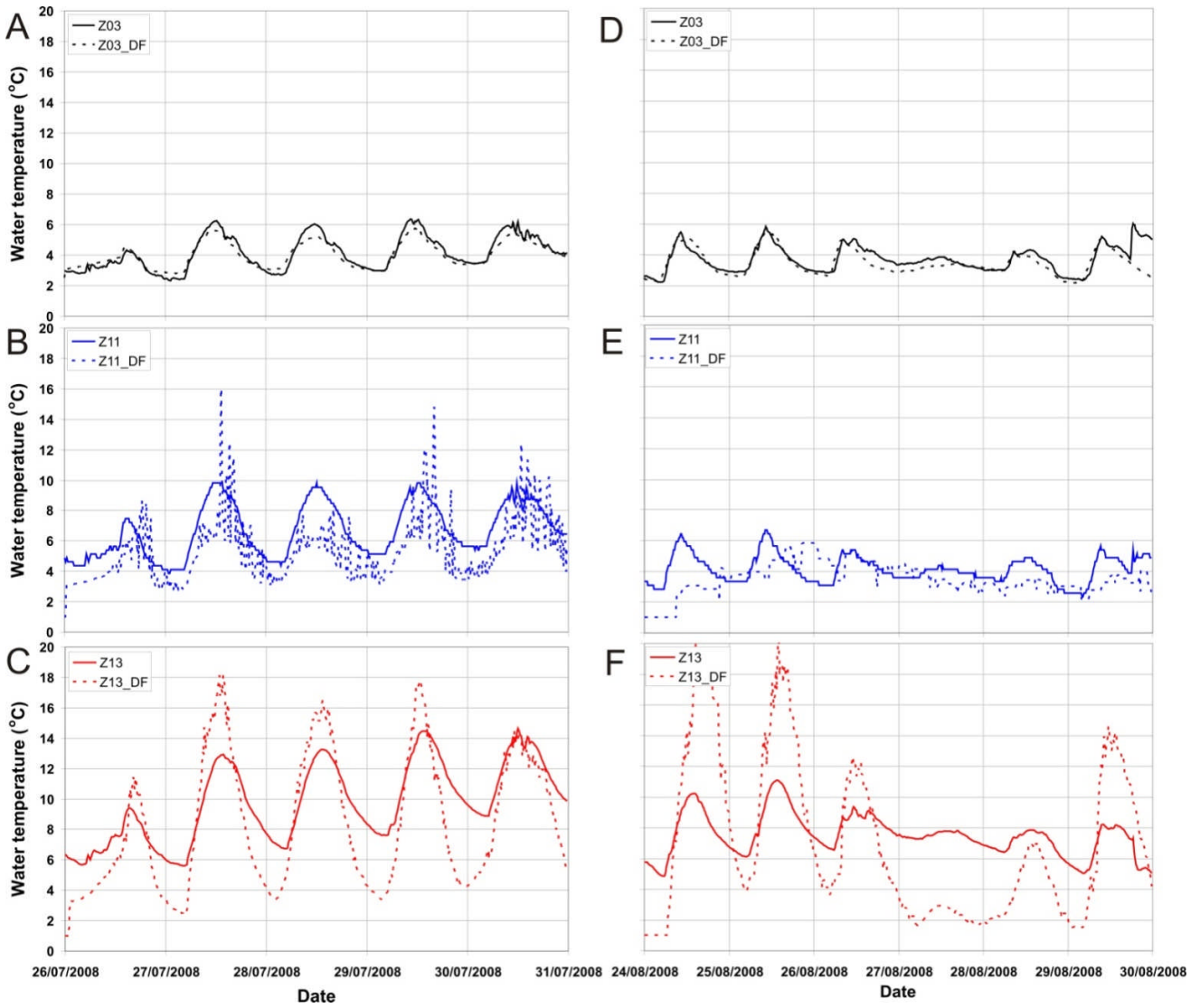


1

2 **Figure 3.** Sensitivity analysis of water temperature to: Turbidity (expressed as ‘Secchi depth’ in Delft  
 3 3D) (A), eddy diffusivity (B), and downstream boundary water temperature (C). This control is  
 4 characterized by an exponential relationship for turbidity (D), an inverse linear relationship for eddy  
 5 diffusivity (E) and an exponential relationship for downstream boundary temperature (F).

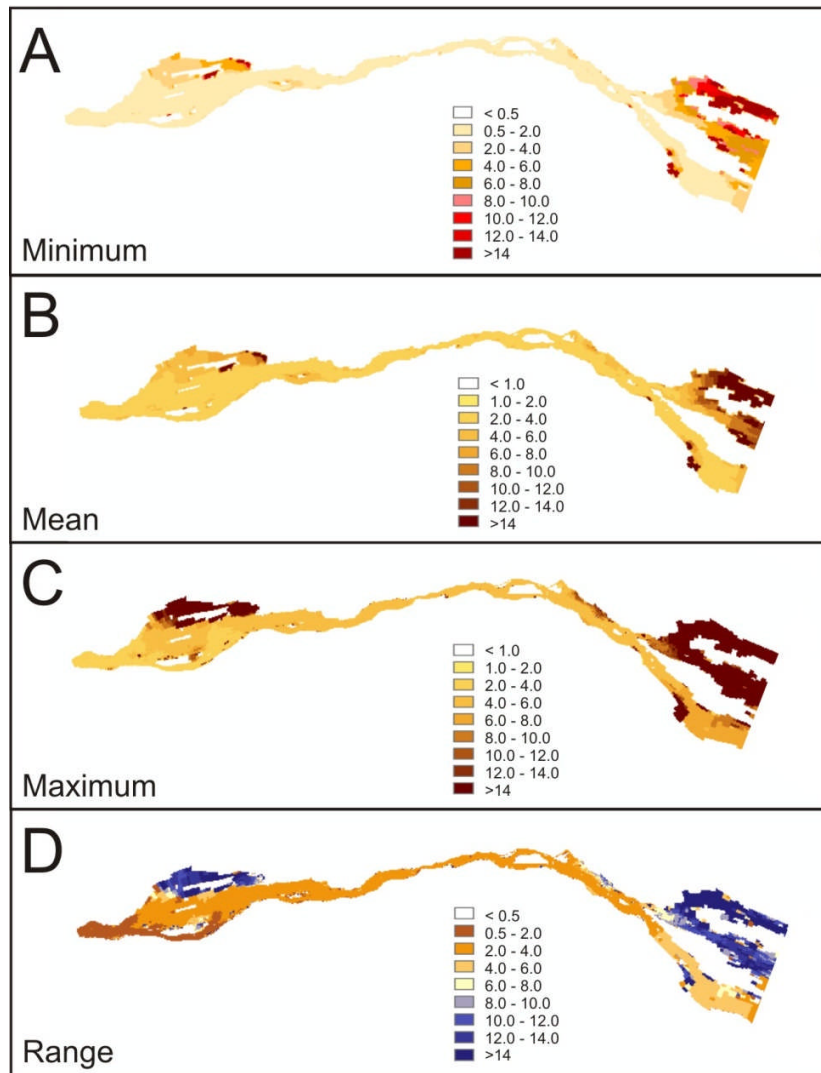
6

7



1  
2  
3  
4  
5  
6  
7  
8  
9  
10  
11  
12

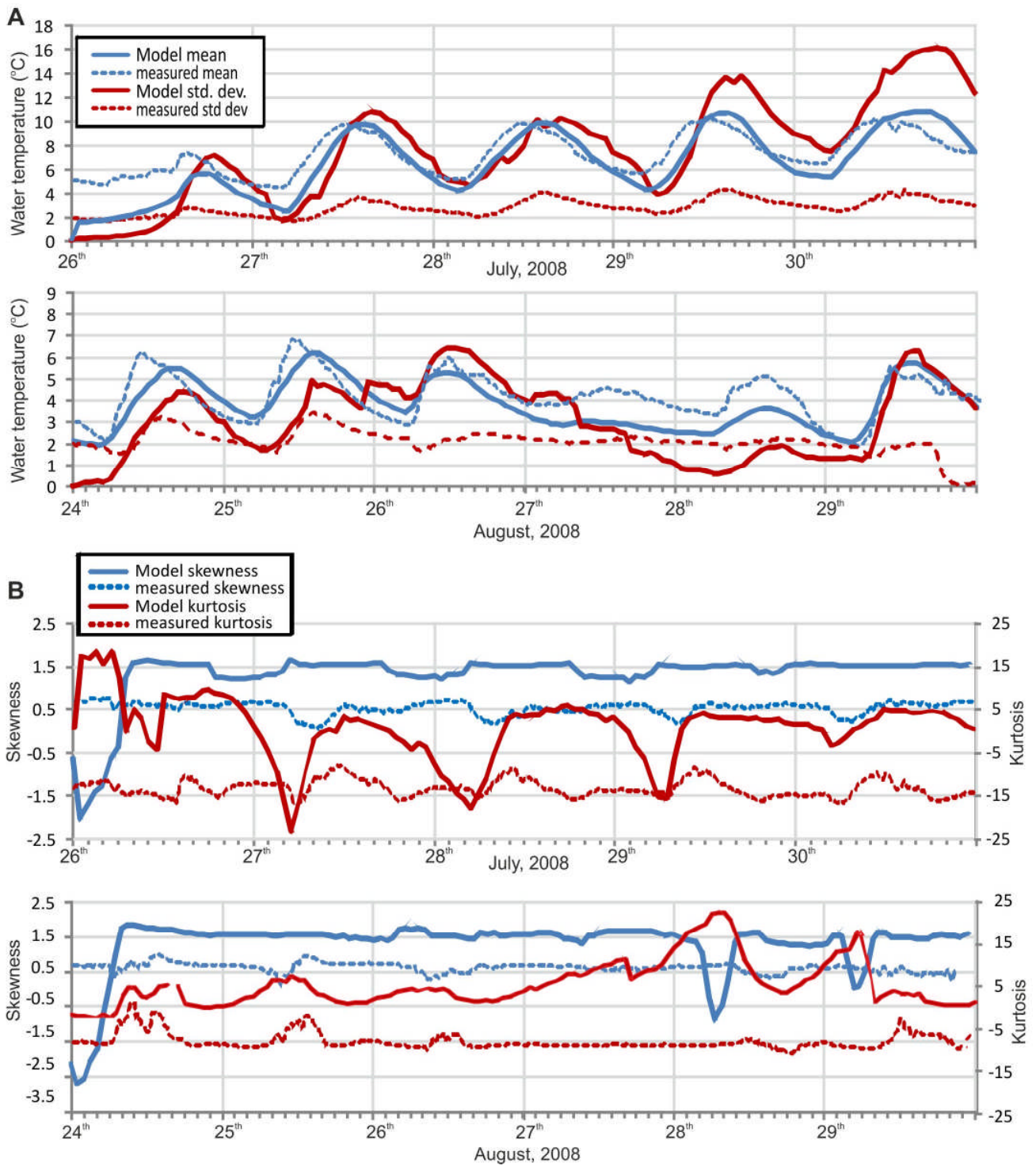
**Figure 4.** Time series of monitored (solid lines) and modelled (dashed lines) water temperature for a main stream channel site (Z03), a site on braided channel (Z11), and a site on the lateral margins of the river network (Z13) for time period one 26-30 July 2008 (A, B, and C respectively), and for time period two 24-29 August, 2008 (D, E and F, respectively).



1  
2  
3  
4  
5  
6  
7  
8  
9

10 **Figure 5.** Spatial distribution of modelled water temperature for time period 1, illustrating the daily  
11 minimum (A), mean (B), maximum (C) and range (D) value for each mesh cell.

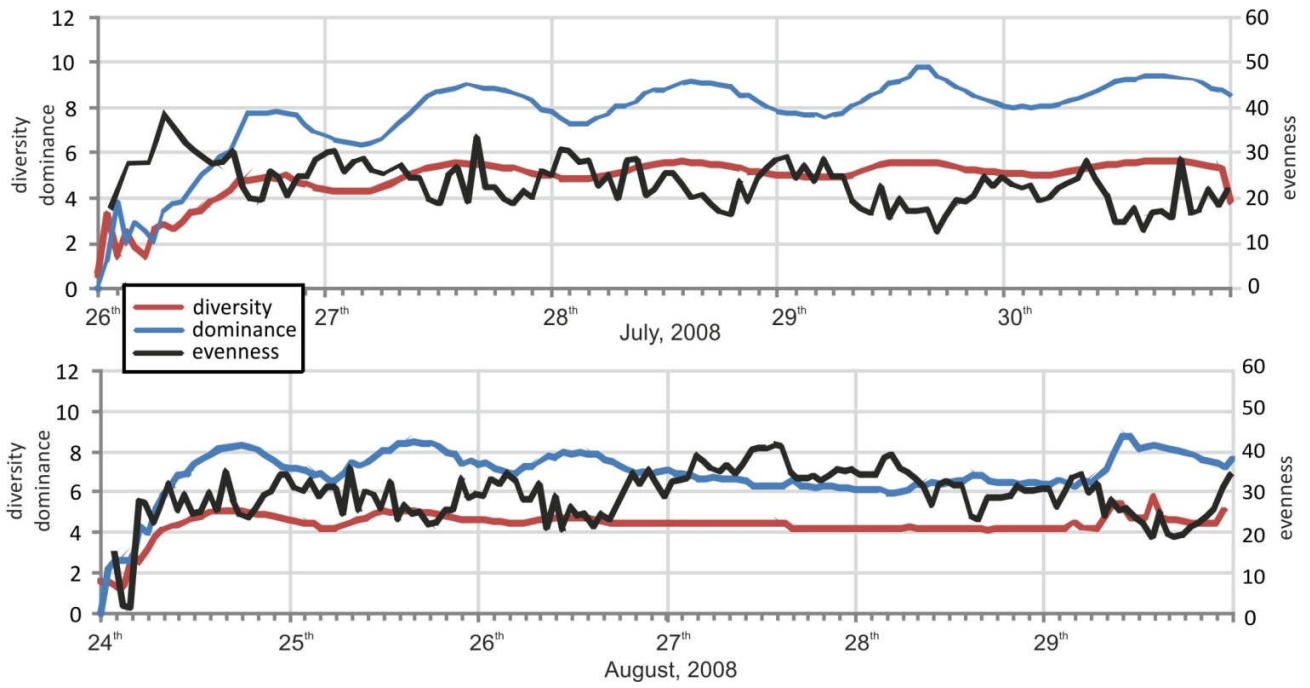
1



2

3

4 **Figure 6.** Temporal distribution of modelled and measured water temperature heterogeneity for both  
5 time periods, illustrating the hourly mean and standard deviation (A), and the hourly skewness and  
6 kurtosis (B). The model results are of all wetted mesh cells; i.e. for the whole model domain.



1

2

3 **Figure 7.** Spatial heterogeneity indices calculated per hour for modelled water temperature model  
 4 representations for all wetted mesh cells; i.e. across the whole model domain.

5

1 **Table 1.** Goodness of fit statistics to assess model performance for each time period, using > 500  
 2 measured and modelled values. The mesh cell at point Z08 was not inundated in the model. All *r* values  
 3 are statistically significant at a 95% confidence interval.

<b>Model time period 1: 26<sup>th</sup> – 31<sup>st</sup> July, 2008</b>							
Site position	Site name	Max. obs-pred (°C)	Min. obs-pred (°C)	ME (°C)	RMSE (°C)	<i>r</i> (-)	Cross corr. mins. ( <i>r</i> )
Main channel	Z02	5.1	0	2.1	2.4	0.89	+ 15 (0.95)
	Z03	0.9	-0.6	0.1	0.3	0.97	+ 0 (0.97)
	Z04	1.3	-0.6	0.2	0.5	0.96	+ 0 (0.96)
	Z06	1.6	-0.6	0.4	0.6	0.96	+ 0 (0.96)
Mid-braidplain	Z05	5.7	-0.2	1.9	2.2	0.90	+ 45 (0.95)
	Z07	2.2	-0.2	1.0	1.1	0.95	+ 30 (0.96)
	Z11	4.1	-6.3	1.4	2.0	0.72	+ 45 (0.95)
Marginal channel	Z08	-	-	-	-	-	-
	Z10	5.1	-8.2	-0.5	3.4	0.71	+90 (0.85)
	Z13	13.8	-5.3	1.4	2.8	0.88	+75 (0.95)

<b>Model time period 2: 24<sup>th</sup> – 30<sup>th</sup> August 2008</b>							
Site position	Site name	Max. obs-pred (°C)	Min. obs-pred (°C)	ME (°C)	RMSE (°C)	<i>R</i> (-)	Cross corr. mins. ( <i>r</i> )
Main channel	Z02	3.0	-1.2	0.8	1.2	0.83	+ 15 (0.89)
	Z03	2.7	-0.7	0.2	0.6	0.76	+ 15 (0.85)
	Z04	2.3	-1.6	-0.3	0.6	0.77	+ 15 (0.86)
	Z06	2.3	-1.6	-0.2	0.6	0.81	+ 0 (0.81)
Mid-braidplain	Z05	3.8	-2.3	0.9	1.5	0.79	+ 60 (0.90)
	Z07	2.4	-1.7	0.3	0.6	0.85	+ 60 (0.90)
	Z11	4.6	-12.2	-1.9	3.8	0.34	+ 90 (0.42)
Marginal channel	Z08	-	-	-	-	-	-
	Z10	10.8	-11.3	0.1	5.9	0.18	+ 30 (0.36)
	Z13	5.6	-10.5	0.3	4.2	0.74	+ 30 (0.76)

4  
 5  
 6  
 7  
 8  
 9  
 10  
 11  
 12  
 13